How the Anti-(Metal Chelate) Antibody CHA255 Is Specific for the Metal Ion of Its Antigen: X-ray Structures for Two Fab′/Hapten Complexes with Different Metals in the Chelate‡

Robert A. Love,*,§ J. Ernest Villafranca,§ Robert M. Aust,§ Kevin K. Nakamura,‖ Rodney A. Jue,‖ Joseph G. Major, Jr.,‖ R. Radhakrishnan,‖ and William F. Butler‖

Agouron Pharmaceuticals, Inc., and Hybritech Incorporated, San Diego, California 92121

Received March 31, 1993; Revised Manuscript Received June 30, 1993®

ABSTRACT: Antibodies with bound metal-chelate haptens provide new means for exploiting the diverse properties of metallic elements. The murine monoclonal antibody CHA255 (IgG1λ) binds the metal-chelate hapten indium(III)-4-[*N*′-(2-hydroxyethyl)thioureido]-L-benzyl-EDTA (designated In-EOTUBE) with high affinity (K_a = 1.1 × 10^{10} M^{-1}). Antibody binding is highly specific for the indium chelate; the affinity decreases as much as 10^4 with other metals, even those having ionic radii close to indium. To better understand this selectivity, the crystal structure of the antigen-binding fragment (Fab′) of CHA255 complexed with its hapten, In(III)-EOTUBE, was determined by molecular replacement and refined at 2.2-Å resolution. The structure of CHA255 Fab′ complexed with Fe(III)-EOTUBE was also determined and refined at 2.8-Å resolution. In both structures, the hapten's EDTA moiety is half-buried near the center of the complementarity-determining regions (CDR's). Five of the six CDR's on the Fab′ interact with the hapten through protein side-chain atoms (but not main-chain atoms). A novel feature of the In-EOTUBE/Fab′ complex is coordination of the indium by Nε of one histidine from the heavy chain's third CDR (distance = 2.4 Å). The histidine coordination is not observed in the Fe-EOTUBE/Fab′ complex, due mainly to a slightly different hapten conformation that reduces metal accessibility; this may partially explain the 20-fold lower affinity of CHA255 for iron hapten. An unexpected feature of the Fab′ overall is an elbow angle of 193° (the angle between the pseudodyad axes of the Fab's constant and variable domains).

Antibodies that bind metal-chelate haptens have many potential uses in medicine. For medical imaging and therapy, hybrid bispecific antibodies can localize the chelate (containing a radioisotope) at a specific target such as a cell surface. In addition to these passive roles for chelate haptens, there are possibilities for more active, chemical roles, e.g., as a cofactor for catalytic antibodies [for review see Lerner *et al.* (1991)]. In any case, a structural understanding of chelate hapten recognition can help in designing or improving a desired chelate/antibody system.

CHA255 is a murine monoclonal antibody of the IgG1λ type. It is the result of immunization with a derivative of the metal chelate In(III)-L-benzyl-EDTA.[1] CHA255 binds a series of derivatives of this chelate, including the hapten used for this study, In(III)-EOTUBE, which is indium(III)-4-[*N*′-(2-hydroxyethyl)thioureido]-L-benzyl-EDTA. A hybrid bispecific antibody was recently prepared that recognizes the EOTUBE hapten with one binding site and tumor-associated antigen CEA with the other (Phelps *et al.*, 1990). This antibody allows the hapten to accumulate preferentially at CEA-bearing tumor sites. The indium functions in this case as a γ-radiation source (^{111}In), with radioimaging applications.

Binding parameters for metal-L-benzyl-EDTA haptens with CHA255, where the metal is varied, have been extensively studied (Reardan *et al.*, 1985). The binding constant is K_a = 4.0 × 10^9 M^{-1} with indium, but decreases as much as 10^4 for other metals, even for trivalent ions with ionic radii close to that of indium. For example, CHA255 binds Fe(III)-L-benzyl-EDTA with K_a = 1.8 × 10^8 M^{-1} despite an ionic radius for iron only 0.17 Å smaller than indium. Similar affinity ratios are observed using metal-EOTUBE haptens, with affinities overall being slightly higher. In-EOTUBE has an affinity of K_a = 1.1 × 10^{10} M^{-1} (Stemmer *et al.*, 1993). To explore the structural basis for the fine discrimination of metal chelates by an antibody, complexes of CHA255 Fab′ with EOTUBE were crystallized and studied by X-ray crystallography.

METHODS

Monoclonal antibodies were the result of (i) immunization with the *p*-thioureido derivative of the metal chelate In(III)-L-benzyl-EDTA conjugated to keyhole limpet hemocyanin, (ii) hybridoma production, and (iii) screening by radioimmunoassay for ability to bind ^{111}In-L-benzyl-EDTA (Reardan *et al.*, 1985). The high-affinity IgG1λ monoclonal antibody CHA255 was selected and purified from mouse ascites fluid. Antibodies were digested with pepsin to generate F(ab′)$_2$ fragments that were subsequently purified by hydrophobic

‡ The coordinates for the two Fab/hapten structures have been deposited in the Brookhaven Protein Data Bank under the entry names 1IND and 1INE.

* To whom correspondence should be addressed.

§ Agouron Pharmaceuticals, Inc.

‖ Hybritech Incorporated.

® Abstract published in *Advance ACS Abstracts,* September 1, 1993.

[1] Abbreviations: Fab, antigen-binding fragment of the antibody; C and V, constant and variable domains, respectively, of the Fab; C_L and C_H, light and heavy chains, respectively, of the constant domain; V_L and V_H, light and heavy chains, respectively, of the variable domain; CDR, complementarity-determining region; Lm, light chain CDR*m*, where *m* = 1, 2, or 3; Hn, heavy chain CDR*n*, where *n* = 1, 2, or 3; Fab′, same as Fab but having additional residues at the carboxy end of the C_H chain; rms, root mean square; σ, standard deviation; CEA, carcinoembryonic antigen; MR, molecular replacement; F_o and F_c, observed and model-calculated structure factors, respectively; ϕ_c, phase angles calculated from an atomic model; *B*-factor, isotropic individual atomic temperature factor; *R*-factor, $\Sigma_{hkl}||F_o| - |F_c||/\Sigma_{hkl}|F_o|$; EDTA, ethylenediaminetetraacetate; EOTUBE, 4-[*N*′-(2-hydroxyethyl)thioureido]-L-benzyl-EDTA.

0006-2960/93/0432-10950$04.00/0

interaction chromatography. These $F(ab')_2$ fragments were mildly reduced with cysteine and alkylated with iodoacetamide to generate Fab' fragments. One Fab' has a relative molecular mass of 48 500, with 442 amino acids.

CHA255 Fab' was incubated with In(III)-EOTUBE or Fe(III)-EOTUBE in a 1:1.5 ratio and then crystallized using hanging-drop vapor diffusion at room temperature. A factorial method was used to search for optimum crystallization conditions (Carter *et al.*, 1988). The best crystals were obtained as follows. Initially, in a 10-μL drop were 5 mg/mL protein, 10% PEG 4000, 0.1 M $CaCl_2$, and 50 mM HEPES (pH 7.5). The well solution had double these amounts (except for protein).

Thin plates of maximum size 0.6 × 0.6 × 0.2 mm were obtained after several weeks. When crystals were washed and analyzed by nondenaturing gel electrophoresis, the presence of the complex Fab'/EOTUBE could be demonstrated (charge is introduced by the hapten). All Fab'-bound EOTUBE should contain chelated metal, based on prior observation of negligible apo-EOTUBE binding (Reardan *et al.*, 1985) as well as the extremely high affinity of EDTA for metals. Vapor diffusion attempts with the Fab' alone did not produce crystals.

The Fab'-hapten crystals belong to space group $C2$ with either In-EOTUBE or Fe-EOTUBE as the hapten, these two cases being nearly isomorphous. The unit cell dimensions are a = 99.3 Å, b = 84.6 Å, c = 76.7 Å, and β = 136.2° for Fab'/In-EOTUBE and a = 99.9 Å, b = 85.6 Å, c = 77.5 Å, and β = 136.4° for Fab'/Fe-EOTUBE. There is one molecule per asymmetric unit, giving a calculated solvent content of 48% for the unit cell. X-ray diffraction was observed as far as 2.0 Å from the best crystals, and one gave substantial data to 2.2 Å, but most crystals provided fairly complete data only to 2.8 Å. Data were collected at room temperature using a dual-chamber area detector system of the Xuong–Hamlin design. Data collection strategies of Xuong *et al.* (1985) were used, including the measurement of each Bijvoet pair within a short time interval (for the iron case).

For Fab'/In-EOTUBE, three crystals provided a 2.8-Å data set that was used during initial analysis. A single crystal later provided the high-resolution data used in atomic refinement, with a ratio of observations to unique reflections of 3.0. Of the 22 000 possible unique reflections to 2.2 Å, 99% have been measured; 81% have intensities $I > 2\sigma(I)$ to 2.5 Å; and 50%, 45%, and 37% have $I > 2\sigma(I)$ in the last three 0.1 Å wide shells, respectively. The average signal-to-noise ratio $\langle I/\sigma(I)\rangle$ is 2.0 at 2.5 Å, dropping to 1.3 for the last shell at 2.3–2.2 Å. The overall R_{merge} on intensity is 9.4% ($=\sum_i|I_i - \langle I\rangle|/\sum\langle I\rangle$, where $\langle I\rangle$ is the average of observed equivalents). From two Fab'/Fe-EOTUBE crystals, of the 10 900 possible unique reflections to 2.8 Å, 81% have been measured and 77% have $I > 2\sigma(I)$. The overall R_{merge} is 7.0% for these two crystals.

From these diffraction data alone, attempts were made to locate the bound hapten's metal ion, to provide an independent reference point during subsequent analysis. A difference Patterson map (to 3 Å) between the indium data and iron data, and a Bijvoet difference Patterson map (to 4 Å) based on the iron hapten anomalous scattering, shared the same highest nonorigin peak (data not shown). Thus the position of the metal could be deduced, aside from the y-coordinate and choice of origin (monoclinic case), this (x,z) position being similar for iron and indium.

Molecular replacement (MR) was pursued using several Fab models from the Brookhaven Protein Data Bank, including KOL (Marquart *et al.*, 1980), NEWM (Saul *et al.*, 1978), McPC603 (Satow *et al.*, 1986), J539 (Suh *et al.*, 1986), R19.9 (Lascombe *et al.*, 1989), HyHEL-5 (Sheriff *et al.*, 1987), HyHEL-10 (Padlan *et al.*, 1989), 4-4-20 (Herron *et al.*, 1989), and B13I2 (Stanfield *et al.*, 1990). Two strategies were employed: (1) dividing each structure into its constant (C) and variable (V) domains, as suggested by Cygler and Anderson (1988), because of the large variation in elbow angle among Fab's; (2) varying the elbow angle within one whole Fab structure to generate a family of search models, as described by Brunger (XPLOR manual).

MR Method (1). All side chains were retained, except that the CDR residues were removed from V models. All of the C models were then aligned to one another, as were the V models, so that common MR solutions could be detected for each domain type. Each C or V model was used in the rotation function of MERLOT (Fitzgerald, 1988), with data 10–4 Å from the Fab'/In-EOTUBE crystals. The most frequent rotation solution among the V models was usually the top solution for each model; a similar result occurred for C models. An example of results for the KOL model follows: Using its C domain, the top rotation solution had a height 5.6 times the rms of the map and was 1.2 rms above the next solution. With its V domain, these numbers are 6.2 and 1.2. Each C or V model was then rotated into its most probable orientation (the most frequent rotation solution for that domain type).

To refine the relative positions of the light and heavy chains within each C or V domain prior to a translation search, the program INTREF (Yeates & Rini, 1990) was employed, using data 10–4 Å and Patterson cutoff radius 24 Å. This led to relative rotational changes up to 4°, and relative translational movements up to 2 Å, between light and heavy chains. The INTREF-refined domains gave more interpretable translation search results.

Using the rotation search and Patterson-correlation (PC) method (Brunger, 1990) provided in XPLOR (Brunger *et al.*, 1987), and the same starting C and V models, we obtained final orientations and relative chain positions nearly identical to those found from MERLOT/INTREF.

The correctly oriented and INTREF (or PC) refined C/V models were used in the XPLOR correlation coefficient translation function. Only an (x,z) search was needed initially for this monoclinic case; 10–4-Å data were used, with a search grid of 1 Å. Convincing solutions were found for C and V models. For example, with a C model derived from KOL, the top solution was 6.1σ above the mean and 4σ above the next solution. With a V model derived from KOL, these numbers were 6.7σ and 4σ. No other orientation (alternate rotation solution) of C or V gave a clear translation solution, even after INTREF or PC refinement. Finally, the y-translation of C with respect to V was determined (by fixing V arbitrarily at y = 0.0); this top solution was 4.5σ above the mean and 3σ above the next solution.

On the basis of the MR results, the C and V coordinates from Fab KOL were used extensively for further analysis. This C+V combination formed a reasonable whole-Fab model and packed into the unit cell without overlaps between symmetry-related molecules. Also, the expected CDR region of the V model coincided with the independently determined site for the hapten's chelated metal. After rigid-body refinement with XPLOR, the R-factor was 0.45 at 3 Å. But because the Fab displayed an elbow angle (≈193°) outside of the commonly observed range (about 130–180°), another MR strategy was pursued in order to rule out the possibility of artifacts from the individual-domain analysis.

MR Method (2). The elbow angle for the complete HyHEL-5 model was varied from 155° to 218° in steps of 7°. Each trial model was used in XPLOR's rotation search, and the top 100 unique solutions were subjected to rigid-body PC refinement (Brunger, 1990), involving first the entire molecule, then the C and V portions, and finally all four Fab domains. Data were in the range 15–4 Å. The highest final PC value (PC = 0.21, twice the next highest value) resulted from four models with *initial* elbow angles in the range 183–204° . In each of these four cases, the final rigid-body *refined* model showed overall orientation, relative domain orientation/translation, and an elbow angle (≈193°) nearly identical to those in the model obtained earlier (from individual C/V analysis). For initial elbows less than but close to 180°, the PC refinement adjusted the Fab toward a linear configuration, although the PC values were lower. Translation searches using all PC-refined models resulted in a common, unambiguous solution (6σ above next highest) only with those four models having large PC values and an elbow angle of ≈193°, this solution giving a unit cell position nearly identical to that derived from the C/V analysis. The entire PC procedure was repeated with several other Fab models, involving slightly different definitions of the elbow's "hinge", with a similar outcome.

QUANTA (Molecular Simulations, Inc.) was used to automatically substitute the known CHA255 amino acid sequence into the MR models. (Sequential residue numbers of CHA255 are used in this report, but they are referenced to Kabat (1991) whenever possible.) Initial XPLOR refinement, with simulated annealing (SA) via "slow cooling" from 2000 K, lowered the residual to 0.30 on all data to 2.5 Å. The structure was then rebuilt into "omit" electron density maps, using primarily the omit–refine procedure of XPLOR (with SA initially and convential refinement in later stages). The $2F_o - F_c$ maps were examined using FRODO (Jones, 1978) on Evans & Sutherland's PS390 or ESV systems. During this process, the CDR's were built into the model, density being unambiguous for all six CDR loops. Also, residues connecting the V and C domains were located. Further XPLOR refinement reduced the R-factor to 0.25 at 2.2 Å (with an overall isotropic B-factor of 18 Å^2). Additional rebuilding was required for several surface loops, mostly in the constant domain, where density was weak. At positions C_L-144 (Kabat 141) and C_H-147, -149, and -189 (Kabat 149, 151, 194), *cis*-prolines were clearly indicated and inserted. In the heavy chain, electron density is not interpretable for the carboxy-terminal 13 amino acids, thus these residues are assumed to be disordered. In the light chain the first residue and the last three residues are disordered. The disorder includes the interchain disulfide between C_L-214 and C_H-215 (Kabat 214 and 230), even though nonreducing gels suggest that the bond remains intact in the crystals.

The bound hapten was located and constructed as follows. Difference Fourier maps phased on the Fab′ model alone revealed one strong positive peak ($>10\sigma$) near the center of the CDR's, implying the chelated metal. These maps had coefficients of either $2F_{indium} - F_c$ or $F_{indium} - F_{iron}$. This site was identical (in x,z) to that derived from the Patterson maps which do not rely on model phases (see above). With the metal position established, weaker density (but $>2\sigma$) in the $(2F_o - F_c)\phi_c$ map indicated the chelating aceto groups of EDTA, the benzyl group, and the hapten's "tail" (ethanol–thiourea). Starting from the known crystal structures of metal-EDTA complexes (Lind *et al.*, 1964; Agre *et al.*, 1981), a complete model for the hapten EOTUBE was built and fit into density. Figure 1a shows density for the indium hapten.

Atomic refinement of the Fab′/In-EOTUBE complex (3231 non-hydrogen atoms) continued as follows. XPLOR's SA refinement was used via slow cooling from only 1000 K, while the hapten's atoms were kept fixed. TNT (Tronrud *et al.*, 1987), followed by PROLSQ (Hendrickson, 1985), with their solvent parameter corrections, was used to refine atomic positions for the entire complex. Restrained individual B-factor refinement was performed using XPLOR or PROLSQ. Electron density maps were examined, corrections were made, and refinement was repeated from the post-SA stage. A total of 145 water molecules (including three buried at the protein–hapten interface) were ultimately included via an automated search of $(F_o - F_c)\phi_c$ maps for peaks above 3.0σ and at reasonable hydrogen-bonding positions.

The final R-factor for the Fab′/In-EOTUBE model is 0.188, using 14 800 reflections with $I > 2\sigma(I)$ in the range 7–2.2 Å. (R = 0.21 for all data to 2.2 Å.) The rms deviations from ideal bond length, angle, and planarity are 0.017 Å, 2.6°, and 0.008 Å, respectively. A Ramachandran plot for the Fab′ is shown in Figure 2. Average B-factors for main-chain and side-chain atoms are $\langle B \rangle_{main}$ = 15.1 Å^2 and $\langle B \rangle_{side}$ = 16.4 Å^2. For the indium hapten $\langle B \rangle$ = 17.8 Å^2, and for water $\langle B \rangle$ = 28.0 Å^2.

The Fab′/Fe-EOTUBE data were initially treated independently. The MR analysis was repeated in order to confirm an overall Fab′ conformation similar to the indium hapten case. The refined 2.2-Å model discussed above, with hapten and CDR's removed, was then used as a starting point for refining and rebuilding the Fab′/Fe-EOTUBE structure. Figure 1b shows electron density for the iron hapten. The final R-factor is 0.176, using 8270 reflections with $I > 2\sigma(I)$ in the range 7–2.8 Å (R = 0.20 for all data to 2.8 Å). The rms deviations from ideal bond length, angle, and planarity are 0.017 Å, 2.6°, and 0.008 Å, respectively. Average B-factors for main-chain and side-chain atoms are $\langle B \rangle_{main}$ = 14.9 Å^2 and $\langle B \rangle_{side}$ = 16.4 Å^2. For the iron hapten $\langle B \rangle$ = 20.0 Å^2, and for water $\langle B \rangle$ = 22.0 Å^2.

The structures were analyzed in various ways. To determine surface areas, the program MS (Connolly, 1983) was used, with a 1.7-Å probe radius and van der Waals radii based on Polygen's modification of the Bondi (1964) values. INSIGHT (Biosym Technologies) and QUANTA were used for various measurements and visualizations on Silicon Graphics workstations. Crystallographic refinement was performed on a Convex C240. *Ab initio* calculations were performed on the Cray-2 at Eli Lilly & Co., using UniChem from Cray Research, Inc., and Gaussian-90. Structural parameters for the Fab (elbow angle, etc.) were determined using unpublished programs of Daved Freemont and Todd Yeates. The atomic coordinates have been deposited with the Brookhaven Protein Data Bank.

RESULTS

Overall Features of the Fab′ Molecule. The CHA255 Fab′ molecule has an "extended", nearly linear conformation. The smallest angle between pseudodyads of the C and V domains is 167°. However, by convention, an Fab elbow angle is defined with respect to the light and heavy chains, such that a decreasing angle causes V_H and C_H domains to overlap before V_L and C_L. Accordingly, the CHA255 elbow must be defined as 193°. When aligned to other Fab structures, CHA255 clearly bends in the "opposite" direction. This unexpected angle exists without any steric clash between residues of the C and V domains and partially preserves a conserved V_H/C_H

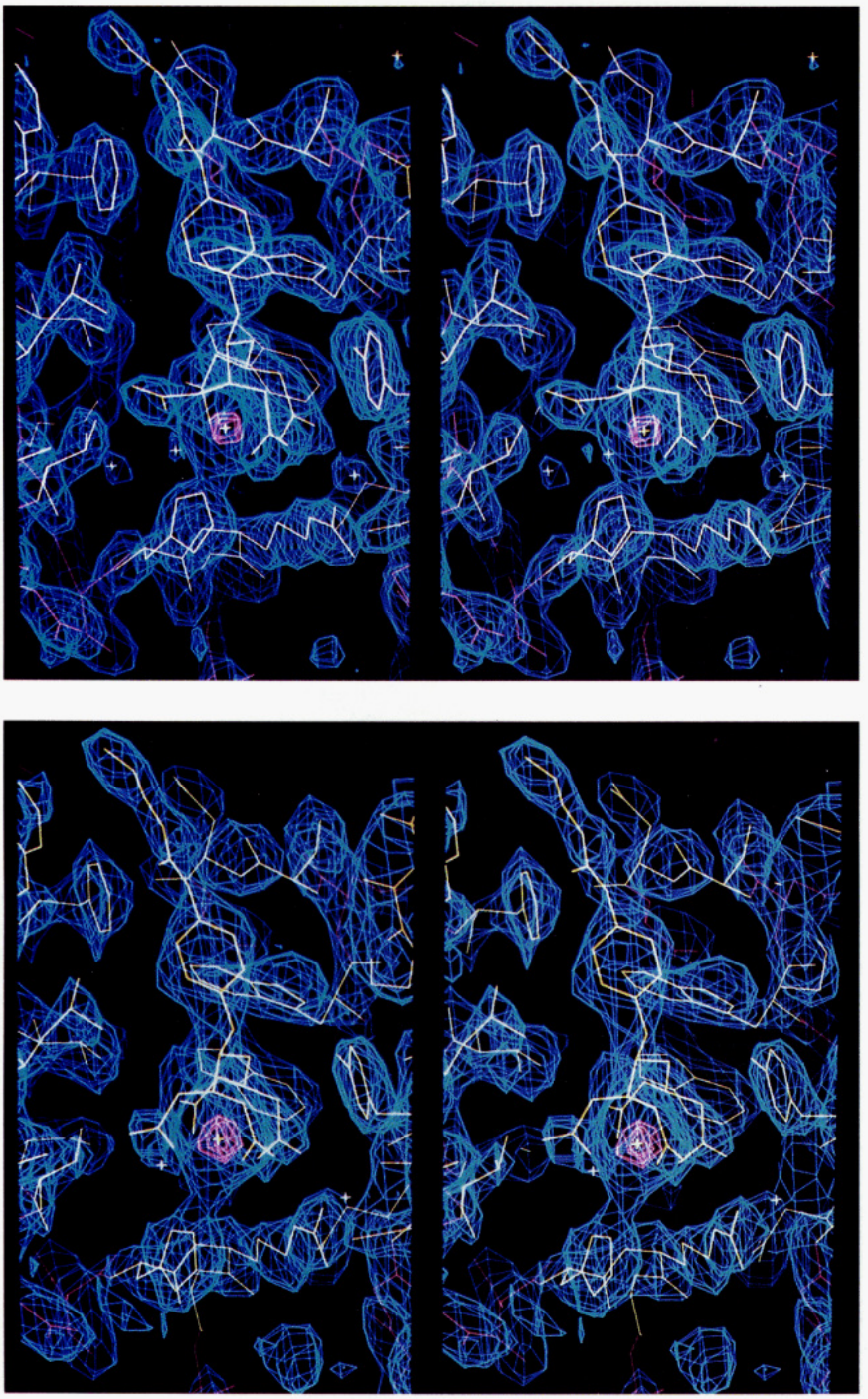

FIGURE 1: $2F_o - F_c$ omit–refine electron density maps in the region of the bound hapten, involving removal of the hapten and all amino acids within 6 Å (yellow). The refined Fab'/hapten coordinates are displayed, and the metal ion is visible within the highest contour level (surrounded by the chelating arms of EDTA). The protein's metal-coordinating residue histidine-99H appears near the bottom of each figure. In (a, top) the hapten is In-EOTUBE, with a 2.2-Å resolution map contoured at 1.2σ (blue) and 12.0σ (violet). In (b, bottom) the hapten is Fe-EOTUBE, with a 2.8-Å resolution map contoured at 1.2σ (blue) and 6.0σ (violet).

interaction observed among Fab's (see Figure 3 and Discussion). Other geometric parameters for CHA255 fall within the observed ranges for Fab structures. V_L and V_H are related by a rotation of 178° and a translation of 0.9 Å. C_L and C_H are related by a rotation of 165° and translation of 2.5 Å. The closest distance between pseudodyads of C and V is 0.35 Å.

The influence of crystal packing, if any, on the elbow angle of CHA255 Fab' is unclear. The molecules lie side-by-side with their long axes approximately parallel, with many intermolecular contacts involving all four subdomains. To address this question, we have recently obtained X-ray data from a different ($P2_1$) crystal form of the Fab'/In-EOTUBE complex, which may reveal an alternate packing arrangement.

Features of the Hapten. During attempts to fit an initial model of EOTUBE into the 2.2-Å electron density maps for Fab'/In-EOTUBE, it became apparent that the bound hapten's chelating arms adopt a configuration closer to that of the Fe-EDTA crystal structure (pentagonal bipyramid geometry; Lind *et al.*, 1964) rather than the In-EDTA structure (capped trigonal prism geometry; Agre *et al.*, 1981). After the EOTUBE model was revised appropriately, the indium coordination distances remained close to those in the In-EDTA structure (within 0.15 Å). Possible explanations for In-EOTUBE's chelate differing from In-EDTA include a different environment for the chelate (bound to an Fab versus being packed in a small molecule crystal lattice) and the fact

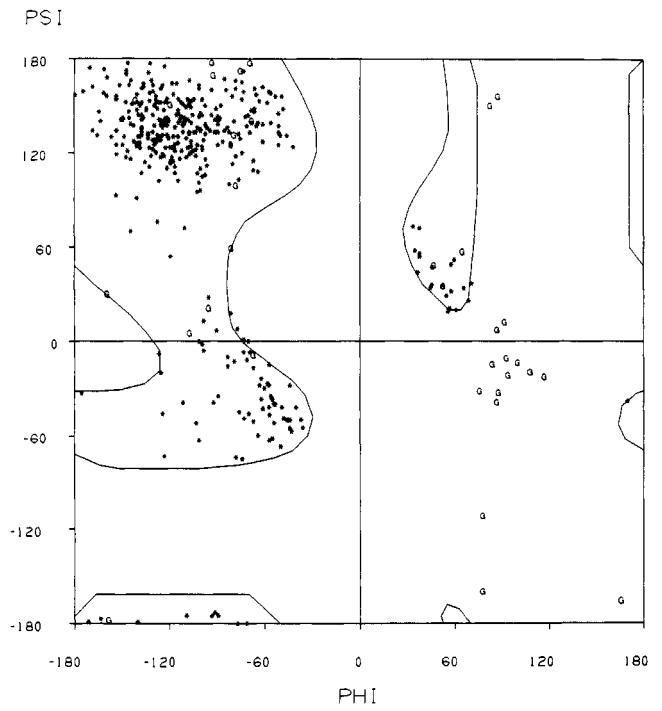

FIGURE 2: Ramachandran plot for the CHA255 Fab′ structure. Non-glycine residues are indicated by an asterisk; glycine residues, by the letter G. Contours represent the $V = 0$ nonbonded energy level for alanine residues (Ramachandran *et al.*, 1966). No (non-glycine) residues lie significantly outside of this contour level.

that EOTUBE's chelate is EDTA with a benzyl substituent on one of the ethylene carbons. In any case, there is evidence for EDTA chelates in solution existing in dynamic equilibrium between several molecular configurations (Kula *et al.*, 1963; Day & Reilley, 1964). For the bound Fe-EOTUBE case, the Fe-EDTA crystal structure fits the hapten density with only minor adjustments, although the resolution for the Fab′/Fe-EOTUBE map is only 2.8 Å.

The crystal structure of EOTUBE alone is unknown. But a conjugate gradient minimization of an In-EOTUBE model incorporating the In-EDTA crystal structure (using XPLOR with estimated CHARMM parameters) suggested a reconfiguration of the EDTA moiety similar to that observed in our complex. In an *ab initio* calculation *in vacuo*, geometry optimizations of In-aminobenzyl-EDTA were performed using the DGauss implementation of density functional theory (Andzelm & Wimmer, 1992; Andzelm, 1991). In these cases the seventh coordination for indium was provided by the ϵ-nitrogen of a methylimidazole moiety. The starting geometries were those from our Fab-bound In-EOTUBE model. The final optimized geometry reflected a pentagonal bipyramidal conformation nearly identical to the starting model. In another, unrelated calculation, using a 3-21G* basis set and GAUSSIAN-90, the plane of the thiourea in EOTUBE was predicted to be 64° from the plane of the benzyl ring, while the observed value is about 56°.

The Hapten Binding Site for In-EOTUBE. A view of the bound hapten In-EOTUBE is shown in Figure 4 and more schematically in Figure 6. The antibody–hapten interface is mostly water-excluding, except for three buried water molecules, two of which mediate hydrogen bonds between the hapten and the protein. The hapten's "head", or EDTA moiety, is half-buried in a major pocket at the center of the CDR's. This pocket is formed solely by CDR amino acids, and all CDR's except L2 have atoms within van der Waals distance (4.1 Å) of the hapten. The interacting residues are summarized in Figure 5, and various bonds at the interface are listed in Table I. There are three hydrogen bonds and one salt link between the hapten and the protein, and two more hydrogen bonds between the hapten and buried waters. The result is that the two relatively buried carboxylate groups of EDTA are hydrogen-bonded to the protein either directly or indirectly through water molecules. EOTUBE's benzyl group lies within a canyon formed mostly by aromatic with a few aliphatic Fab′ side chains. The hapten's "tail" (the thiourea–ethanol) extends farther from the Fab′ surface, probably because the ethanol was not part of the original immunogen, and the thiourea was involved in the lysine–benzyl linkage of that immunogen.

Overall, the EDTA moiety fits very tightly into the hapten site, while direct contacts become fewer in a direction from the benzyl to ethanol. Nevertheless, the entire length of the hapten forms a solvent-excluding interface. The buried surface areas are as follows. With a 1.7-Å probe radius, about 304 Å^2 of EOTUBE (70% of total hapten surface area) and 355 Å^2 of antibody are buried in the complex. The three buried waters improve receptor–ligand complementarity by "filling holes" on the antibody surface. The heavy chain of CHA255 contributes about 56% of the Fab's buried surface area and the light chain about 44%.

In the case of In-EOTUBE, the CDR H3 plays a major role in the Fab′–hapten interaction. H3 interacts primarily through two residues, His-99H and Arg-100H (Kabat 95H and 96H): (i) The His-99H ϵ-nitrogen provides a seventh coordination to the indium atom chelated within the EDTA group, the Nϵ–indium distance being 2.4 Å. In the small molecule crystal structure of In-EDTA, this seventh coordination is provided by the oxygen of a sulfate molecule from the solvent (distance = 2.1 Å). (ii) Arg-100H is ion-paired to one EDTA carboxylate, and the side chain's Nϵ is hydrogen-bonded to an adjacent EDTA carboxylate. In terms of formal charges, there is net neutrality around the hapten: EDTA = −4, indium = +3, and arginine = +1.

The Hapten Binding Site for Fe-EOTUBE. An early difference Fourier map between indium and iron data, phased on the Fab′ model alone (without hapten), had suggested movement of the chelating arms of the EDTA moiety and a large movement of His-99H away from the coordination position, when the hapten is Fe-EOTUBE. Independent refinement of the Fab′/Fe-EOTUBE complex confirms these changes; see Figure 7. Neither nitrogen atom on the imidazole ring of His-99H could lie within 3.6 Å of the iron; thus there is no significant metal coordination. The hapten's chelating arms adopt slightly different dihedral angles and are more constricted about the metal than in In-EOTUBE, such that any coordination attempt by the histidine leads to several carboxylate–imidizole clashes. A few other Fab side-chain positions differ slightly between the two complexes, but higher resolution data for the Fe-EOTUBE case will be needed for a more detailed comparison.

DISCUSSION

The three-dimensional structure of CHA255 Fab′ complexed with its metal-chelating hapten EOTUBE has many features in common with known Fab/hapten structures, yet it also presents a few novel and unexpected results. CHA255 is one of the first λ-light-chain murine Fab structures to be solved and the first Fab/hapten structure showing a direct interaction between an antibody and a metal within its hapten.

While possessing the immunoglobin fold found in all Fab's, and having a typical light–heavy chain relationship within each domain (constant and variable), the 193° elbow angle

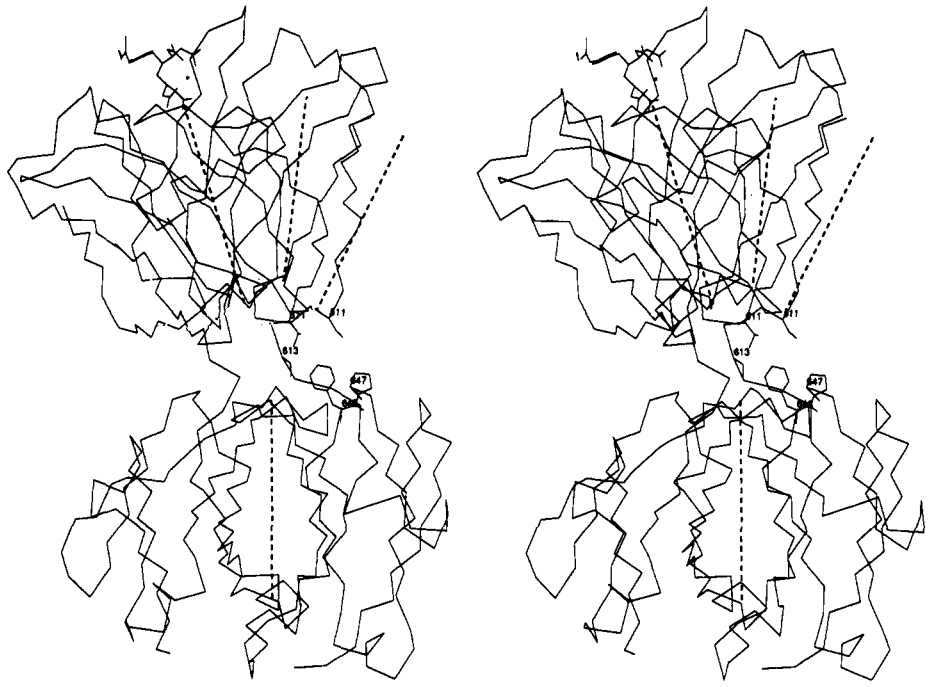

FIGURE 3: Stereoview α-carbon trace of the CHA255 Fab', which has been oriented for maximum emphasis of the elbow bend between constant (bottom) and variable (top) domains. Dashed lines represent the pseudodyad axes for CHA255 and two other Fab's once all are aligned on their constant domains (superimposing light and heavy chains appropriately). The three adjacent dashed lines indicate, from left to right, the variable domain's pseudodyad in CHA255 (elbow = 193°), in KOL (elbow = 167°), and in J539 (elbow = 144°). Residues of CHA255 involved in the postulated "ball and socket" are labeled (see Discussion). The bound hapten is visible near the top of the molecule, its EDTA moiety, near the pseudodyad axis.

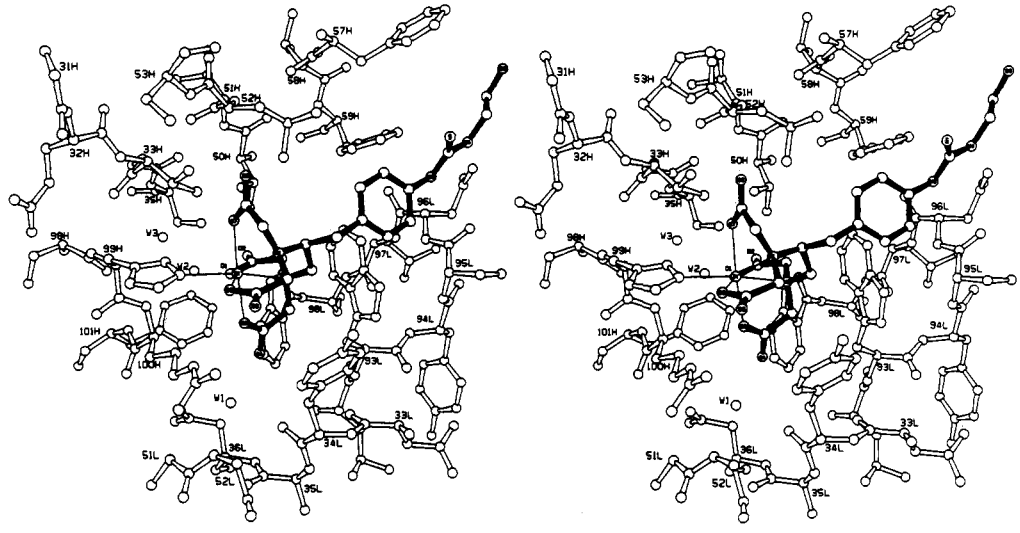

FIGURE 4: Stereoview of the antibody's binding pocket with bound hapten for the CHA255/In-EOTUBE complex. Fab' residues have open bonds, and the hapten has solid bonds. Thin lines indicate the coordination of the indium ion. L denotes light chain, and H denotes heavy chain. The three buried water molecules are labeled W1–W3.

for CHA255 lies outside the usual range of about 130–180°. We are aware of only one other structure with an elbow angle beyond 180°, the unliganded anti-sweetener Fab NC6.8 with 184° (L. W. Guddat and A. B. Edmundson, personal communication). It has been proposed by Lesk and Chothia (1988) that an elbow angle appreciably greater than 180° would disrupt a "ball-and-socket" interaction found in all Fab structures, formed between conserved residues of C_H and V_H. In their model (with Kabat numbering), the V_H residues 11 (Leu, Val, or Phe), 110 (Thr), and 112 (Ser) form a "socket" that rotates on the "ball" composed of C_H residues 148 (Phe or Leu) and 149 (*cis*-Pro). In CHA255 such an interaction is partially preserved, between Ser-11/Thr-111/Ser-113 and Phe-146, but there is an additional rotation of the socket in a direction *perpendicular* to that defining the usual range of elbow angles, causing Pro-147 to lie just outside of the socket (see Figure 3). Whether the CHA255 elbow results from its IgG1λ type or from crystal packing forces remains to be determined. In any case, it now appears that antigen binding and elbow angle are independent phenomena, with the latter due merely to flexibility within the Fab molecule (Davies *et al.*, 1990; Stanfield *et al.*, 1990; Rini *et al.*, 1992).

The CHA255 Fab'/metal-EOTUBE interface (Figure 4) shows the characteristic features of Fab/hapten association, with surface complementarity and nearly total exclusion of water molecules (except for buried waters adding to the complementarity). The general manner of EOTUBE binding parallels that seen in other Fab/hapten structures involving

L1	R	S	S	T	G	A	V	T	T	S	N	**Y**	A	N	
	24	25	26	27	D	E	F	28	29	30	31	32	33	34	Kabat
	23	24	25	26	27	28	29	30	31	32	33	34	35	36	CHA255
L2	G	T	N	N	R	A	P								
	50	51	52	53	54	55	56								
	52	53	54	55	56	57	58								
L3	A	L	**W**	Y	**S**	N	L	**W**	V						
	89	90	91	92	93	94	95	96	97						
	91	92	93	94	95	96	97	98	99						
H1	G	E	**T**	M	S										
	31	32	33	34	35										
	31	32	33	34	35										
H2	T	T	L	**S**	G	G	G	**F**	T	**F**	Y	S	A	S	V	K	G
	50	51	52	A	53	54	55	56	57	58	59	60	61	62	63	64	65
	50	51	52	53	54	55	56	57	58	59	60	61	62	63	64	65	66
H3	H*	**R**	F	V	H										
	95	96	97	98	99										
	99	100	101	102	103										

FIGURE 5: Sequences of CDR residues for the CHA255 antibody (one-letter amino acid code), with the numbering scheme of Kabat et al. (1991) on the top line and the CHA255 linear sequence below. An outlined letter indicates that the residue has atoms within 4.1 Å of the hapten (In-EOTUBE), without any hydrogen bonding. Bold letters are residues which hydrogen-bond to the hapten (always via their side chains). The special case of the histidine which coordinates the hapten's metal is denoted by the asterisk. Underlined letters are residues that hydrogen-bond to the hapten through one of the buried water molecules (in this case both main-chain and side-chain protein atoms are involved). There are no Fab′–hapten interactions involving non-CDR residues.

phosphocholine (Satow *et al.*, 1986), fluorescein (Herron *et al.*, 1989), phenyl arsonate (Strong *et al.*, 1991), and dinitrophenyl spin-label (Brunger *et al.*, 1991) in that the hapten is significantly buried in a pocket formed near the center of the CDR's (near the local 2-fold axis of the V_L–V_H interface). This location on the Fab allows contact with the maximum number of CDR residues and is also employed by (one portion of) polymer haptens such as polypeptides (Stanfield *et al.*, 1990; Rini *et al.*, 1992), oligosaccharides (Cygler *et al.*, 1991), and oligonucleotides (Herron *et al.*, 1991). For CHA255 Fab′, the hapten binding pocket is roughly 10 Å by 15 Å wide and 6 Å deep and is occupied primarily by the benzyl-EDTA portion of the ligand. A shallow trough along the V_L–V_H interface provides contacts for the remaining tail of the ligand.

The buried surface areas on CHA255 Fab′ and its hapten EOTUBE (355 and 304 Å^2, respectively) are most similar to the Fab/fluorescein complex (308 and 266 Å^2 for antibody and hapten), the Fab/oligosaccharide complex (304 and 255 Å^2 for antibody and hapten), and the Fab/dinitrophenyl complex (350 and 232 Å^2 for antibody and hapten) while about double the Fab/phosphocholine case (161 and 137 Å^2 for antibody and hapten) and much less than the B13I2 Fab/peptide case (540 and 460 Å^2 for antibody and antigen) or the Fab/lysozyme cases (over 700 Å^2 on both lysozyme and its antibody). The contributions from heavy and light chains to buried surface area for CHA255 (56% and 44%, respectively) are about midway between the case of phosphocholine (53%, 47%) and fluorescein (60%, 40%). In terms of percent of total ligand surface area buried in the complex, EOTUBE at 70% falls behind phosphocholine (81%) and fluorescein (94%). Though not as completely buried as these two haptens, EOTUBE is desolvated along its entire length, leading to overall immobilization of the molecule. [Values in this paragraph were taken from Davies *et al.* (1990) and Stanfield *et al.* (1990).]

An examination of the contacts at the Fab′/In-EOTUBE interface reveals many van der Waals interactions, five hydrogen bonds from hapten to either the protein or the buried water, one ion pair, and the histidine–indium coordination. Figure 5 summarizes these interactions with respect to the CDR residues, Figure 6 displays the interactions schematically, and Table I lists the various distances. All the CDR's interact directly with bound EOTUBE except L2; this exception is found frequently in small hapten/Fab structures (Davies *et al.*, 1990; Mian *et al.*, 1991). As in most antibody structures, tryptophan and tyrosine residues play major roles in forming the CHA255 antigen-binding site (Mian *et al.*, 1991). The inventory of bonds in Fab′/EOTUBE is closest to the fluorescein case (six hydrogen bonds to the protein and one ion pair), and similar binding affinities are observed for the two systems ($\sim 1.0 \times 10^{10}$ M^{-1}).

The most unusual feature of the Fab′/In-EOTUBE interaction is the coordination by His-99H (Kabat 95H) to the hapten's indium ion. Metals are typically coordinated 7-fold by EDTA, six atoms coming from the EDTA (four oxygens, two nitrogens) and the seventh from a solvent oxygen (Agre *et al.*, 1981; Lind *et al.*, 1964; Richards *et al.*, 1964). His-99H provides the seventh coordination via the Nϵ on its imidazole. The coordination distance here of 2.4 Å is somewhat longer than the average 2.1 Å seen in most histidine–metal coordinations (Chakrabarti, 1990), but the approach of His-99H is restricted by the chelating carboxylate groups around the metal, as well as protein-induced restraints on the side-chain position. The contribution to binding energy by this coordination is difficult to estimate, but it may partially compensate for the incomplete burial of EOTUBE compared to fluorescein, thus making their affinities approximately equal.

For Fab′-bound Fe-EOTUBE the His-99H coordination does not occur, apparently because the imidazole cannot approach the iron without contacting the relatively more-enveloping carboxylate chelating groups of the EDTA moiety (Figure 7). The EDTA conformation is slightly constricted because of the smaller ionic radius for iron (0.17 Å smaller than indium). Aside from His-99H, Fab′–hapten interactions (and buried surface areas) for Fe-EOTUBE are very similar to the In-EOTUBE case. Therefore, the absence of the histidine coordination may be largely responsible for the 20-fold lower binding affinity of iron hapten to CHA255 (Reardan *et al.*, 1985). Supporting this idea, recent studies in which His-99H was mutated to isoleucine showed a 20-fold lower binding affinity of CHA255 toward In-EOTUBE (Patricia Ahrweiler, personal communication).

More difficult to rationalize are cases in which chelated metals have the same ionic radius as indium or iron and yet CHA255 binding affinities are much lower than for either one (Reardan *et al.*, 1985). A Sc(III) hapten binds to CHA255 with 10^3 lower affinity than the In(III) hapten despite identical ionic radii for scandium and indium. A Co(III) hapten binds to CHA255 with 10^2 lower affinity than the Fe(III) hapten despite identical ionic radii for cobalt and iron. Here it is possible that the EDTA moiety of the bound hapten adopts a configuration different from that which we observe for In-EOTUBE and Fe-EOTUBE (perhaps a capped trigonal prism instead of the pentagonal bipyramid of our structures). This idea is plausible given the multiple conformations known for EDTA chelates in solution (see Results) and would involve a significantly different CHA255–hapten interface, perhaps lacking the metal/His-99H coordination. Further elucidation awaits crystallization of CHA255 Fab′ with chelates containing metals other than indium or iron, or production of new antibodies directed against a non-In-EOTUBE chelate.

In summary, we predict the same *overall* orientation for most metal-EOTUBE haptens bound to CHA255, since

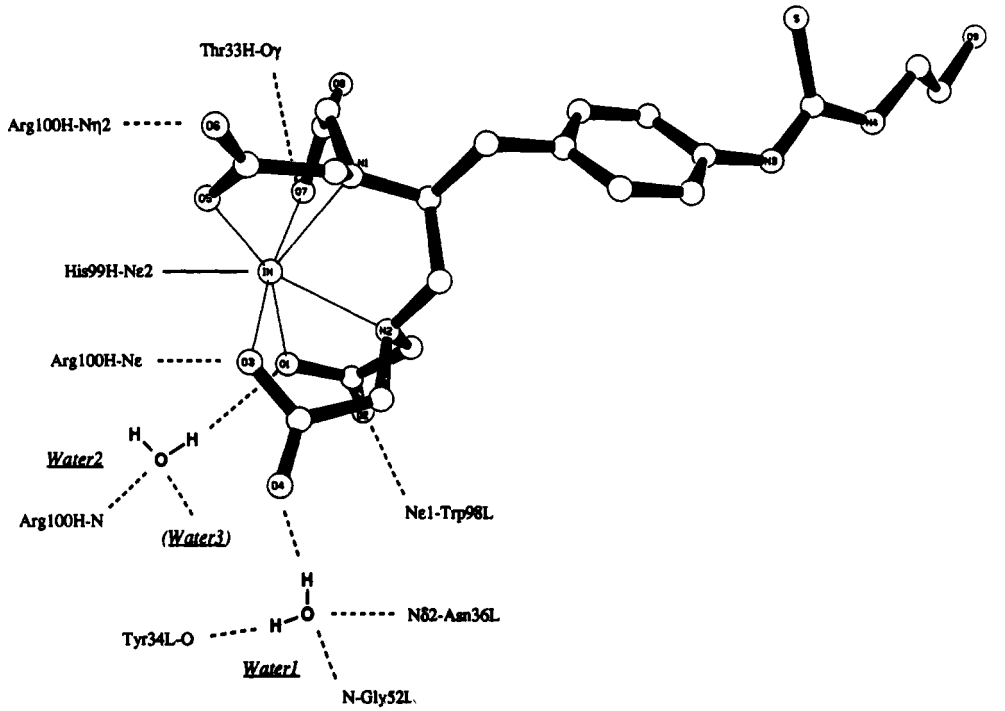

FIGURE 6: View of the bound hapten In-EOTUBE in which the Fab is represented schematically. (Compare with Table I.) Hydrogen bonds from the hapten to the protein or buried water are shown as dashed lines. Coordination of the metal is shown by solid lines. Water3 (not shown for simplicity) forms hydrogen bonds to the protein and Water2 but not to the hapten.

Table I: Interactions at the CHA255 Fab'/In-EOTUBE Interface

donor	acceptor	distance (Å)	type
His-99H Nε2	EOTUBE In^{3+}	2.40	coord[a]
Arg-100H Nη2	EOTUBE O6	3.52	ion pair
Trp-98L Nε1	EOTUBE O2	2.76	hb[b]
Thr-33H Oγ1	EOTUBE O7	3.19	hb
Arg-100H Nε	EOTUBE O3	3.08	hb
water 2	EOTUBE O1	2.74	hb
water 1	EOTUBE O4	2.80	hb
Asn-36L Nδ2	water 1	3.09	hb
Gly-52L N	water 1	2.93	hb
Arg-100H N	water 2	2.85	hb
Ser-35H Oγ	water 3	2.75	hb
water 1	Tyr-34L O	2.78	hb
water 3	Ser-98H O	3.04	hb
water 3	water 2	2.70	hb
EOTUBE O1	EOTUBE In^{3+}	2.31	coord
EOTUBE O3	EOTUBE In^{3+}	2.24	coord
EOTUBE O5	EOTUBE In^{3+}	2.30	coord
EOTUBE O7	EOTUBE In^{3+}	2.33	coord
EOTUBE N1	EOTUBE In^{3+}	2.46	coord
EOTUBE N2	EOTUBE In^{3+}	2.45	coord

[a] Coordination of metal ion. [b] Hydrogen bond.

affinities do exceed 1×10^5 for all metals tested (Reardan *et al.*, 1985). But the detailed interactions between non-indium haptens (i.e., nonimmunogens) and CHA255 should not be optimum, partly because of nonideal coordination between the protein and the chelated metal, as well as potentially different coordination geometry within the hapten's EDTA moiety. An analogous explanation may be applicable to studies in which antibodies distinguish between metals in porphyrin-type antigens (Schwabacher *et al.*, 1989).

The structural findings for Fab'/EOTUBE are consistent with recent biochemical studies of EOTUBE binding to CHA255 antibody (Meyer *et al.*, 1990). Kinetic analysis of In-EOTUBE dissociation suggested that at least one antibody amino acid which changes ionization in the pH 6–8 range (probably histidine) is directly involved in binding. This may correlate with the structure's coordinating residue His-99H, since no other histidine is present in the hapten-binding site.

In the earlier binding study (Reardan *et al.*, 1985), it was found that In-EDTA binds to CHA255 antibody with 24-fold lower affinity than L-benzyl-In-EDTA, implying an important role for the aromatic group that was part of the original immunogen. In our structure, the benzyl moiety makes up a significant portion of the solvent-excluding, buried surface area of EOTUBE. Also in that study it was found that affinity for D-benzyl-EDTA is 70-fold lower than for L-benzyl-EDTA, demonstrating that the stereochemistry of the benzyl substitution is critical. We find that if D-benzyl-EDTA is modeled into the CHA255 Fab' structure, keeping the Fab'–EDTA interactions unchanged, then the benzyl group must point into solution. Thus D-benzyl-EDTA probably has fewer interactions with the Fab' than the L-isomer.

The three-dimensional view of a metal-chelate hapten bound to its antibody can serve as a starting point toward reengineering the complex for many purposes. The current application of the CHA255/EOTUBE system (localization of radioisotopes at a target via bispecific antibodies) could be expanded by structure-based modification of the hapten or the antibody, so that other metals or other chelate derivatives could be employed. The contributions of various antibody–antigen interactions to binding affinity could be explored during these modifications. In other applications, redesign goals might include the replacement of the chelate's metal-coordinating groups (and thus the entire chelate) with antibody residues; this idea has already been explored via remodeling of the anti-fluorescein antibody to create a zinc coordination site in the binding pocket (Roberts *et al.*, 1990; Iverson *et al.*, 1990).

There may also be the potential to develop an active chemical role for a metal-chelate hapten similar to EOTUBE. One approach might be to use the chelate as a chemical cofactor in a reaction catalyzed by the antibody. Sequence-specific proteolysis has already been demonstrated with a catalytic antibody that uses a triethylenetetraamine–metal complex as

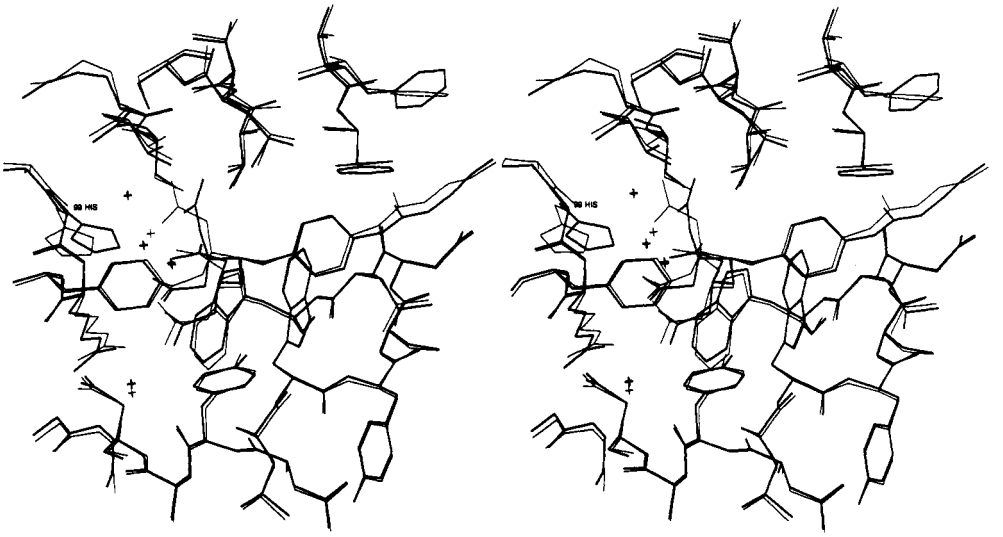

FIGURE 7: Stereoview comparison of the Fab'/Fe-EOTUBE complex (thin lines) with the Fab'/In-EOTUBE complex (thick lines). The primary structural differences are the His-99 side-chain position (seen at left) and the configuration of the hapten's EDTA moiety.

a cofactor, the immunogen consisting of the chelate strategically linked to a peptide (Iverson & Lerner, 1989). Several other examples exist in which an elicited antibody has adjacent binding sites for substrate and chelate cofactor, with a spatial relationship sufficient for reactivity (Lerner *et al.*, 1991).

Finally, given the known ability of Fe-EDTA to cleave oligonucleotides (Dervan, 1986) and polypeptides (Rana & Meares, 1990, 1991) via a metal-bound hydroxide, another application of a chelate-hapten/antibody might be localization of this general hydrolytic function at a specific target via a bispecific antibody. There is precedence for an EDTA-catalyzed reaction attaining site-specific, enzyme–substrate character, when the EDTA is first attached to a molecule that binds another selectively, for example, studies of oligonucleotide–EDTA complexed with DNA (Moser & Dervan, 1987) and (DNA-binding) protein–EDTA complexed with DNA (Sluka *et al.*, 1987). In the antibody/chelate case, an EDTA-type hapten might function whether or not it first dissociated from the antibody.

REFERENCES

Agre, V. M., Kozlova, N. P., Trunov, V. K., & Ershova, S. D. (1981) *Zh. Strukt. Khim. 22*, 138–146.

Andzelm, J. (1991) in *Density Functional Methods in Chemistry* (Labanowski, J., & Andzelm, J., Eds.) Springer-Verlag, New York.

Andzelm, J., & Wimmer, E. (1992) *J. Chem. Phys. 96*, 1280–1303.

Bondi, A. (1964) *J. Phys. Chem. 68*, 441–451.

Brunger, A. T. (1990) *Acta Crystallogr. A46*, 46–57.

Brunger, A. T., Kurian, J., & Karplus, M. (1987) *Science 235*, 458–460.

Brunger, A. T., Leahy, D. J., Hynes, T. R., & Fox, R. O. (1991) *J. Mol. Biol. 221*, 239–256.

Carter, C., Baldwin, E., & Frick, L. (1988) *J. Cryst. Growth 90*, 60–73.

Chakrabarti, P. (1990) *Protein Eng. 4*, 57–63.

Connolly, M. L. (1983) *Science 221*, 709–713.

Cygler, M., & Anderson, W. F. (1988) *Acta Crystallogr. A44*, 38–45, 300–308.

Cygler, M., Rose, D. R., & Bundle, D. R. (1991) *Science 253*, 442–445.

Davies, D. R., Padlan, E. A., & Sheriff, S. (1990) *Annu. Rev. Biochem. 59*, 439–473.

Day, R. J., & Reilley, C. N. (1964) *Anal. Chem. 36*, 1073–1076.

Dervan, P. B. (1986) *Science 232*, 464–470.

Fitzgerald, P. M. D. (1988) *J. Appl. Crystallogr. 21*, 273–278.

Hendrickson, W. A. (1985) in *Methods in Enzymology* (Wyckoff, H. W., Hirs, C. H. W., & Timasheff, S. N., Eds.) Vol. 115, pp 252–270, Academic Press, New York.

Herron, J. N., He, X., Mason, M. L., Voss, E. W., & Edmundson, A. B. (1989) *Proteins: Struct., Funct., Genet. 5*, 271–280.

Herron, J. N., He, X. M., Ballard, D. W., Blier, P. R., Pace, P. E., Bothwell, A. L. M., Voss, E. W., & Edmundson, A. B. (1991) *Proteins 11*, 159–175.

Iverson, B. L., & Lerner, R. A. (1989) *Science 243*, 1184–1188.

Iverson, B. L., Iverson, S. A., Roberts, V. A., Getzoff, E. D., Tainer, J. A., Benkovic, S. J., & Lerner, R. A. (1990) *Science 249*, 659–662.

Jones, T. A. (1978) *J. Appl. Crystallogr. 11*, 268–272.

Kabat, E. A., Wu, T. T., Reid-Miller, M., Perry, H. M., Gottesman, K. S., & Foeller, C. (1991) *Sequences of Proteins of Immunological Interest*, 5th ed., National Institutes of Health, Bethesda, MD.

Kula, R. J., Sawyer, D. T., Chan, S. I., & Finley, C. M. (1963) *J. Am. Chem. Soc. 85*, 2930–2936.

Lascombe, M. B., Alzari, P. M., Boulot, G., Saludjian, P., Tougard, P., Berek, C., Haba, S., Rosen, E. M., Nisonoff, A., & Poljak, R. J. (1989) *Proc. Natl. Acad. Sci. U.S.A. 86*, 607–611.

Lerner, R. A., Benkovic, S. J., & Schultz, P. G. (1991) *Science 252*, 659–667.

Lesk, A. M., & Chothia, C. (1988) *Nature 335*, 188–190.

Lind, M. D., Hamor, J. H., Hamor, T. A., & Hoard, J. L. (1964) *Inorg. Chem. 3*, 34–44.

Marquart, M., Deisenhofer, J., Huber, R., & Palm, W. (1980) *J. Mol. Biol. 141*, 369–391.

Meyer, D. L., Fineman, M., Unger, B. W., & Frincke, J. M. (1990) *Bioconjugate Chem. 1*, 278–284.

Mian, I. S., Bradwell, A. R., & Olson, A. J. (1991) *J. Mol. Biol. 217*, 133–151.

Moser, H. A., & Dervan, P. B. (1987) *Science 238*, 645–650.

Padlan, E. A., Silverton, E. W., Sheriff, S., Cohen, G. H., Smith-Gill, S. J., & Davies, D. R. (1989) *Proc. Natl. Acad. Sci. U.S.A. 86*, 5938–5942.

Phelps, J. L., Beidler, D. E., Jue, R. A., Unger, B. W., & Johnson, M. J. (1990) *J. Immunol. 145*, 1200–1204.

Ramachandran, G. N., Venkatachalam, C. M., & Krimm, S. (1966) *Biophys. J. 6*, 849–872.

Rana, T., & Meares, C. F. (1990) *J. Am. Chem. Soc. 112*, 2457–2458.

Rana, T., & Meares, C. F. (1991) *J. Am. Chem. Soc. 113*, 1859–1861.

Reardan, D. T., Meares, C. F., Goodwin, D. A., McTigue, M., David, G. S., Stone, M. R., Leung, J. P., Bartholomew, R. M., & Frincke, J. M. (1985) *Nature 316*, 265–267.

Richards, S., Pedersen, B., Silverton, J. V., & Hoard, J. L. (1964) *Inorg. Chem. 3*, 27–34.

Rini, J. M., Schulze-Gahmen, U., & Wilson, I. A. (1992) *Science 255*, 959–965.

Roberts, V. A., Iverson, B. L., Iverson, S. A., Benkovic, S. J., Lerner, R. A., Getzoff, E. D., & Tainer, J. A. (1990) *Proc. Natl. Acad. Sci. U.S.A. 87*, 6654–6658.

Satow, Y., Cohen, G. H., Padlan, E. A., & Davies, D. R. (1986) *J. Mol. Biol. 190*, 593–604.

Saul, F. A., Amzel, L. M., & Poljak, R. J. (1978) *J. Biol. Chem. 253*, 585–597.

Schwabacher, A. W., Weinhouse, M. I., Auditor, M.-T. M., & Lerner, R. A. (1989) *J. Am. Chem. Soc. 111*, 2344–2346.

Sheriff, S., Silverton, E. W., Padlan, E. A., Cohen, G. H., Smith-Gill, S. J., Finzel, B. C., & Davies, D. R. (1987) *Proc. Natl. Acad. Sci. U.S.A. 84*, 8075–8079.

Sluka, J. P., Horvath, S. J., Bruist, M. F., Simon, M. I., & Dervan, P. B. (1987) *Science 238*, 1129–1132.

Stanfield, R. L., Fieser, T. M., Lerner, R. A., & Wilson, I. A. (1990) *Science 248*, 712–719.

Stemmer, W. P. C., Morris, S. K., & Wilson, B. S. (1993) *BioTechniques 14*, 256–265.

Strong, R. K., Campbell, R., Rose, D. R., Petsko, G. A., Sharon, J., & Margolies, M. N. (1991) *Biochemistry 30*, 3739–3757.

Suh, S. W., Bhat, J. N., Navia, M. A., Cohen, G. H., Rao, D. N., Rudikoff, S., & Davies, D. R. (1986) *Proteins: Struct., Funct., Genet. 1*, 74–80.

Tronrud, D. E., Ten Eyck, L., & Matthews, B. W. (1987) *Acta Crystallogr. A43*, 489–501.

Xuong, N. H., Nielsen, C., Hamlin, R., & Anderson, D. (1985) *J. Appl. Crystallogr. 18*, 342–350.

Yeates, T. O., & Rini, J. M. (1990) *Acta Crystallogr. A46*, 352–359.